Effects of switching frequency and leakage inductance on slow-scale stability in a voltage controlled flyback converter*

Wang Fa-Qiang(王发强)† and Ma Xi-Kui(马西奎)

State Key Laboratory of Electrical Insulation and Power Equipment, School of Electrical Engineering, Xi'an Jiaotong University, Xi'an 710049, *China*

(Received 13 February 2013; revised manuscript received 6 May 2013)

The effects of both the switching frequency and the leakage inductance on the slow-scale stability in a voltage controlled flyback converter are investigated in this paper. Firstly, the system description and its mathematical model are presented. Then, the improved averaged model, which covers both the switching frequency and the leakage inductance, is established, and the effects of these two parameters on the slow-scale stability in the system are analyzed. It is found that the occurrence of Hopf bifurcation in the system is the main reason for losing its slow-scale stability and both the switching frequency and the leakage inductance have an important effect on this slow-scale stability. Finally, the effectiveness of the improved averaged model and that of the corresponding theoretical analysis are confirmed by the simulation results and the experimental results.

Keywords: flyback converter, slow-scale stability, improved averaged model, Hopf bifurcation

PACS: 05.45.–a, 84.30.Jc, 45.10.Hj **DOI:** 10.1088/1674-1056/22/12/120504

1. Introduction

The flyback converter, whose structure is simpler than those of other types of DC–DC converter such as Buck converter, Boost converter, Buck–Boost converter, and forward converter, is widely used in the field of low power applications. Especially, due to its topology which includes the transformer, it is easy to obtain the multiple output port to supply the different levels of the output voltage.[1] Thus, many researchers make much effort to investigate the operational principle, explore the design methodology, establish the appropriate model, and design the appropriate controller for the flyback converter, and a great number of good results have been obtained.[1–8] However, the complex nonlinear phenomena in the flyback converter are seldom concerned in the existing literature. Until now, there have been only a few typical studies.[9,10] For example, Hsieh *et al*. studied the complex nonlinear phenomena in the UC3842 current programmed flyback converter by using the discrete model and pointed out that the period-doubling bifurcation and chaos could be observed when its input voltage decreased.[9] Xie *et al.* investigated the period-doubling bifurcation and border collision in the voltage controlled flyback converter. Based on the piece-wise discrete map, the period-1, period-2, period-3, period-4, period-5, period-8, and chaos in this converter were analyzed theoretically and confirmed by the circuit experiment.[10] But, the above two important studies only focused on the fast-scale instability, which is often caused by the period-doubling bifurcation occurring at the switching frequency, in the flyback converter. The slow-scale instability, which is regarded as a kind of low-frequency instability, has been rarely concerned in the flyback converter. However, according to the research results about the slow-scale instability in the voltage controlled non-isolated DC–DC converter,[11–14] the pulse train controlled non-isolated DC–DC converter,[15] the one cycle controlled non-isolated DC–DC converter,[16] the current controlled non-isolated DC–DC converter,[17–21] it is easy to obtain the conclusion that the current stress of the switch in the converter increases seriously and it is hard to design the appropriate input filter to remove it. In other words, the occurrence of slow-scale instability in the non-isolated DC–DC converter would bring the disadvantageous effects on the performance of the system, and it is not being accepted in practical engineering. To our knowledge, comparing with the non-isolated DC–DC converter, the topology of the flyback converter is essentially different since it includes a real transformer, and accordingly the existing results about slow-scale instability investigations and the corresponding analysis on the non-isolated DC–DC converter cannot be directly applied to the flyback converter. Namely, it is necessary to investigate the slow-scale stability in the flyback converter renewably and completely, especially to analyze the effects of the key parameters such as the leakage inductance and the switching frequency on this low frequency stability, and give its stability boundaries to present the guidance for designing this converter in practical engineering.

*Project supported by the National Natural Science Foundation of China (Grant No. 51007068), the Specialized Research Fund for the Doctoral Program of Higher Education, China (Grant No. 20100201120028), the Natural Science Basic Research Plan in Shaanxi Province, China (Grant No. 2012JQ7026), the Fundamental Research Funds for the Central Universities, China (Grant No. 2012jdgz09), and the Fund from the State Key Laboratory of Electrical Insulation and Power Equipment, China (Grant No. EIPE12303).

†Corresponding author. E-mail: faqwang@mail.xjtu.edu.cn

© 2013 Chinese Physical Society and IOP Publishing Ltd

Generally, the slow-scale stability in the DC–DC converter can be analyzed by establishing a discrete model or an averaged model. For the discrete model, its main idea is to solve the differential equations derived from the DC–DC converter in each state and then sample the circuit variables at a fixed time. This model is usually used to analyze the slow-scale stability accurately.[11–14] But, its tedious theoretical derivations lead to its limitation in practice. For the averaged model, its main ideal is to average each circuit variable within one switching period and it is effective to use this model to analyze the slow-scale stability approximately.[18,19] But, since its expression in the previous work did not cover the switching frequency, the effect of the switching frequency on the slow-scale stability cannot be analyzed. Additionally, for the voltage controlled flyback converter in practice, the leakage inductance of the real transformer is not zero and it is inevitable to affect on the slow-scale stability of the system which needs to be considered seriously. Therefore, it is still necessary to explore the appropriate model, which covers both the switching frequency and the leakage inductance, to analyze their effect on the slow-scale stability in the system completely.

The rest of the paper is organized as follows. In Section 2, the system description and its mathematical model are briefly reviewed. Then, in Section 3, the improved averaged model of the system, which covers both the switching frequency and the leakage inductance, is established and analyzed theoretically. The stability boundaries in the parameter spaces of the switching frequency versus the leakage inductance are given. In Section 4, the effectiveness of the improved averaged model and that of the corresponding theoretical analysis are confirmed by the simulation results and the experimental results. Finally, some concluding remarks and comments are given in Section 5.

2. System description and its mathematical model

The circuit schematic diagram of the voltage controlled flyback converter is shown in Fig. 1(a). It consists of a flyback converter and a voltage controller. For the flyback converter, it includes an input voltage $V_{\rm in}$, a transformer with a turn ratio between the primary and secondary windings $N_{\rm p}:N_{\rm s}$, the primary winding inductance $L_{\rm m}$ with the leakage inductance $L_{\rm e}$, a switch S implemented by means of a MOSFET, a diode D, a capacitor C, and a load R. For the voltage controller, it includes a voltage divider, a voltage compensator and a PWM comparator. Note that the ground of the output voltage of the flyback converter is different from the ones of the input voltage and the voltage controller. Thus, a voltage sensor VSEN should be inserted to measure the output voltage v_0.

By considering that the transformer is non-ideal, its circuit model can be replaced by the ideal transformer with two inductors.[22] One inductor has an inductance equal to the primary winding inductance $L_{\rm m}$ and the other has the leakage inductance $L_{\rm e}$. The corresponding equivalent circuit model of the system is shown in Fig. 1(b). Note that only the continuous conduction mode (CCM) in the system is concerned in this paper and the circuit parameters are chosen to be $V_{\rm in}=10$ V, $L_{\rm m}=3.05$ mH, $N=N_{\rm p}/N_{\rm s}=100/50$, $C=22.4$ μF, $R=50$ Ω, $R_{\rm vi}=10$ kΩ, $R_{\rm vd}=2$ kΩ, $V_{\rm ref}=1.6$ V, $R_{\rm vf}=10$ kΩ, $C_{\rm vf}=0.47$ μF, $V_{\rm L}=0$ V, and $V_{\rm U}=4$ V.

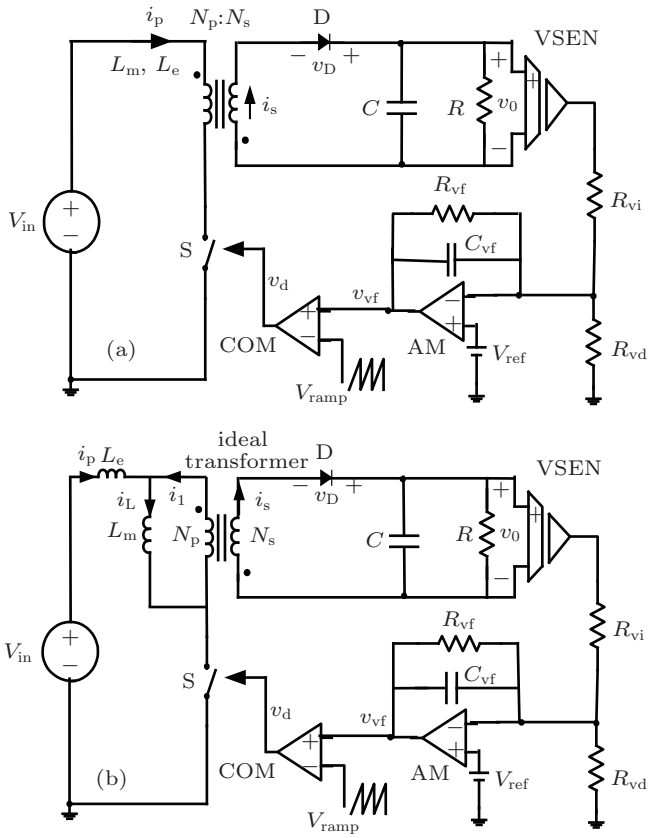


Fig. 1. Circuit schematics of the voltage controlled flyback converter of (a) the origin circuit and (b) the equivalent circuit.

2.1. Flyback converter description

In order to see the operation state of the flyback converter clearly, the typical time-domain waveforms for current $i_{\rm L}$, current $i_{\rm p}$, current i_1, voltage $v_{\rm D}$, and PWM signal $v_{\rm d}$ for $f=30$ kHz and $L_{\rm e}=168$ μH are given in Fig. 2. Note that if $v_{\rm d}=0$, the switch S is in OFF state. But, when $v_{\rm D}=0$ the diode is in ON state. According to the states of the switch S and the diode D within one switching period, there are three topologies, which are called configurations $\rm M_1$, $\rm M_2$, and $\rm M_3$ with corresponding durations about d_1T, d_2T, and d_3T, respectively. Moreover, $d_1T+d_2T+d_3T=T$.

The configuration $\rm M_1$ (OFF, ON) is given when the switch S is in OFF state and the diode D is in ON state. The

current $i_{\rm p}$ is zero and the inductor $L_{\rm m}$ transfers its energy to the load. Accordingly, the current $i_{\rm L}$ equals i_1 and their values both decrease.

The configuration M_2 (ON, ON) is given when the switch S changes from the OFF state to the ON and the diode D remains in ON state, and the inductor $L_{\rm m}$ still transfers its energy to the load. But, for the nonzero leakage inductance $L_{\rm e}$, the current $i_{\rm p}$ increases from zero gradually, i.e., it takes some time to make the current $i_{\rm p}$ equal $i_{\rm L}$, which implies the current $i_{\rm s}$ is zero. In other words, this configuration will not exist when the leakage inductance $L_{\rm e}$ of the transformer is zero, i.e., $L_{\rm e}=0$. What is more important is that as soon as the current $i_{\rm p}$ equals $i_{\rm L}$, the flyback converter operates in configuration M_3 immediately.

The configuration M_3 (ON, OFF) is given when the switch S remains in ON state and the diode D changes to OFF state for its adverse voltage. Thus, only the capacitor C transfers energy to the load. Additionally, the source transfers energy to the inductor $L_{\rm e}$ and $L_{\rm m}$ by increasing their currents ($i_{\rm p}$ and $i_{\rm L}$) linearly.

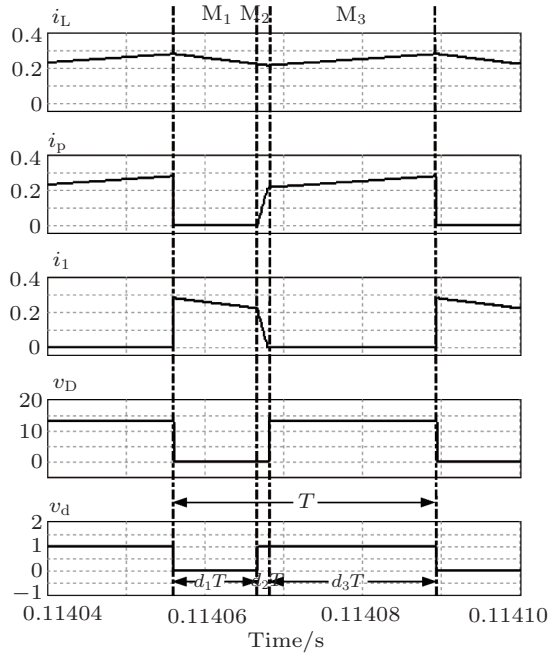


Fig. 2. Typical time-domain waveforms of the flyback converter for $f=30$ kHz and $L_{\rm e}=168$ μH.

From the above configurations, the switched model, which is a basic model for deriving the averaged model, can be derived by using the Kirchhoff's voltage law and the Kirchhoff's current law. Therefore, the inductor current $i_{\rm L}$, the current $i_{\rm p}$, and the voltage v_0 are chosen to be the system's variables.

1) For configuration M_1 (OFF, ON)

$$\begin{cases} \dfrac{{\rm d}i_{\rm L}}{{\rm d}t} = -\dfrac{N}{L_{\rm m}}v_0, \\ \dfrac{{\rm d}v_0}{{\rm d}t} = \dfrac{Ni_{\rm L}}{C} - \dfrac{v_0}{RC}, \\ i_{\rm p} = 0. \end{cases} \tag{1}$$

2) For configuration M_2 (ON, ON)

$$\begin{cases} \dfrac{{\rm d}i_{\rm L}}{{\rm d}t} = -\dfrac{N}{L_{\rm m}}v_0, \\ \dfrac{{\rm d}v_0}{{\rm d}t} = \dfrac{N}{C}(i_{\rm L}-i_{\rm P}) - \dfrac{v_0}{RC}, \\ \dfrac{{\rm d}i_{\rm p}}{{\rm d}t} = \dfrac{V_{\rm in}+Nv_0}{L_{\rm e}}. \end{cases} \tag{2}$$

3) For configuration M_3 (ON, OFF)

$$\begin{cases} \dfrac{{\rm d}i_{\rm L}}{{\rm d}t} = \dfrac{V_{\rm in}}{L_{\rm m}+L_{\rm e}}, \\ \dfrac{{\rm d}v_0}{{\rm d}t} = -\dfrac{v_0}{RC}, \\ \dfrac{{\rm d}i_{\rm p}}{{\rm d}t} = \dfrac{V_{\rm in}}{L_{\rm m}+L_{\rm e}}. \end{cases} \tag{3}$$

2.2. Voltage controller description

The objective of the voltage controller is to adjust appropriately the duty ratio to regulate the output voltage to satisfy the requirements in engineering applications. Among the techniques of the popular voltage compensators, the first-order low pass filter technique is considered here and its mathematical model can be derived as follows:

$$\frac{{\rm d}v_{\rm vf}}{{\rm d}t} = \left(\frac{1}{R_{\rm vf}}+\frac{1}{R_{\rm vi}}+\frac{1}{R_{\rm vd}}\right)\frac{V_{\rm ref}}{C_{\rm vf}} - \frac{v_{\rm vf}}{C_{\rm vf}R_{\rm vf}} - \frac{v_0}{R_{\rm vi}C_{\rm vf}}, \tag{4}$$

where $v_{\rm vf}$ is the output voltage of voltage controller and $V_{\rm ref}$ is the reference voltage.

The state of switch S is determined by comparing the voltage $v_{\rm vf}$ with the ramp signal $V_{\rm ramp}$, whose expression is described by

$$V_{\rm ramp} = V_{\rm L} + (V_{\rm U}-V_{\rm L})\left(\frac{t}{T} \bmod 1\right), \tag{5}$$

where $V_{\rm L}$ and $V_{\rm U}$ are the lower and the upper threshold of the ramp signal, and T is the switching period. The switch S turns on when $v_{\rm con} > V_{\rm ramp}$, and turns off when $v_{\rm con} < V_{\rm ramp}$.

In the previous work, the leakage inductance $L_{\rm e}$ is seldom concerned since its value is very small compared with the primary inductance $L_{\rm m}$. Also, the switching frequency f is seldom concerned for its absence of the existed averaged model which is very popular in the analyzing and designing process. However, the leakage inductance $L_{\rm e}$ and the switching frequency f are two important parameters in the designing process of the flyback converter, so that it is necessary to establish an appropriate model which covers these two parameters to analyze their effects on the dynamical behaviors of the system, which is given in the next section.

3. Improved averaged model derivations and theoretical analysis

In order to analyze the effects of the switching frequency f and the leakage inductance L_e on the slow-scale stability in the voltage controlled flyback converter, in general, the averaged model should be established. However, from the existing literature, the absence of the above two parameters in the previous averaged model leads to no way to analyze their effects.

Based on Eqs. (1)–(5), the averaged model can be directly derived by averaging the circuit variables within one switching period.

$$\begin{cases} \dfrac{\mathrm{d}\langle i_L\rangle}{\mathrm{d}t} = -\dfrac{N}{L_m}\langle v_0\rangle\left(1-\dfrac{\langle v_{vf}\rangle}{V_m}+d_2\right) \\ \qquad\qquad +\dfrac{V_{in}}{L_m+L_e}\left(\dfrac{\langle v_{vf}\rangle}{V_m}-d_2\right), \\ \dfrac{\mathrm{d}\langle v_0\rangle}{\mathrm{d}t} = \dfrac{N}{C}\langle i_L\rangle\left(1-\dfrac{\langle v_{vf}\rangle}{V_m}+d_2\right) \\ \qquad\qquad -\dfrac{N}{C}\langle i_p\rangle d_2-\dfrac{\langle v_0\rangle}{RC}, \\ \dfrac{\mathrm{d}\langle v_{vf}\rangle}{\mathrm{d}t} = \left(\dfrac{1}{R_{vf}}+\dfrac{1}{R_{vi}}+\dfrac{1}{R_{vd}}\right)\dfrac{V_{ref}}{C_{vf}} \\ \qquad\qquad -\dfrac{\langle v_{vf}\rangle}{C_{vf}R_{vf}}-\dfrac{\langle v_0\rangle}{R_{vi}C_{vf}}, \end{cases} \tag{6}$$

where $\langle i_L\rangle$, $\langle v_0\rangle$, $\langle v_{vf}\rangle$, and $\langle i_p\rangle$ are the averaged values of i_L, v_0, v_{vf}, and i_p respectively, and V_m is the peak-to-peak value of the ramp signal V_{ramp}.

According to the geometric relationships between the current i_L and i_p, the following equations can be derived:

$$\langle i_p\rangle = \langle i_L\rangle(d-d_2)+\frac{V_{in}+N\langle v_0\rangle}{2fL_e}d_2^2. \tag{7}$$

By inserting Eq. (7) into Eq. (6), the following equations can be obtained:

$$\begin{cases} \dfrac{\mathrm{d}\langle i_L\rangle}{\mathrm{d}t} = -\dfrac{N}{L_m}\langle v_0\rangle\left(1-\dfrac{\langle v_{vf}\rangle}{V_m}+d_2\right) \\ \qquad\qquad +\dfrac{V_{in}}{L_m+L_e}\left(\dfrac{\langle v_{vf}\rangle}{V_m}-d_2\right), \\ \dfrac{\mathrm{d}\langle v_0\rangle}{\mathrm{d}t} = \dfrac{N\langle i_L\rangle}{C}\left(1-\dfrac{\langle v_{vf}\rangle}{V_m}(1+d_2)+d_2+d_2^2\right) \\ \qquad\qquad -\dfrac{Nd_2^3}{C}\dfrac{V_{in}+N\langle v_0\rangle}{2fL_e}-\dfrac{\langle v_0\rangle}{RC}, \\ \dfrac{\mathrm{d}\langle v_{vf}\rangle}{\mathrm{d}t} = \left(\dfrac{1}{R_{vf}}+\dfrac{1}{R_{vi}}+\dfrac{1}{R_{vd}}\right)\dfrac{V_{ref}}{C_{vf}} \\ \qquad\qquad -\dfrac{\langle v_{vf}\rangle}{C_{vf}R_{vf}}-\dfrac{\langle v_0\rangle}{R_{vi}C_{vf}}. \end{cases} \tag{8}$$

Furthermore, by using the averaging method for the current i_L within one switching period, the following equation can be obtained:

$$\langle i_L\rangle-\frac{V_{in}}{2f(L_m+L_e)}\left(\frac{\langle v_{vf}\rangle}{V_m}-d_2\right)=\frac{V_{in}+N\langle v_0\rangle}{L_ef}d_2. \tag{9}$$

Thus, the following key expression can be obtained:

$$d_2=\frac{(2f\langle i_L\rangle(L_m+L_e)V_m-V_{in}\langle v_{vf}\rangle)L_e}{(2L_mV_{in}+2(L_m+L_e)N\langle v_0\rangle+L_eV_{in})V_m}. \tag{10}$$

Note that $L_e=0$ implies $d_2=0$ and $\langle i_p\rangle=\langle i_L\rangle d$, which satisfy the derivations for the ideal transformer case. Thus, the improved averaged model of the voltage controlled flyback converter can be obtained by combing Eq. (8) with Eq. (10). Obviously, this model, which is for a continuous nonlinear system and its stability and the bifurcation type can be identified by observing the calculated eigenvalues of the Jacobian matrix at its equilibrium point, covers both the switching frequency f and the leakage inductance L_e, so that their effects on the dynamical behaviors of system can be analyzed.

The equilibrium point of the improved averaged model can be calculated by making the terms on the right-hand side of Eq. (8) be zero, i.e.,

$$\begin{cases} -\dfrac{N}{L_m}V_0\left(1-\dfrac{V_{vf}}{V_m}+D_2\right)+\dfrac{V_{in}}{L_m+L_e}\left(\dfrac{V_{vf}}{V_m}-D_2\right)=0, \\ \dfrac{NI_L}{C}\left(1-\dfrac{V_{vf}}{V_m}(1+D_2)+D_2+D_2^2\right) \\ -\dfrac{ND_2^3}{C}\dfrac{V_{in}+NV_0}{2fL_e}-\dfrac{V_0}{RC}=0, \\ \left(\dfrac{1}{R_{vf}}+\dfrac{1}{R_{vi}}+\dfrac{1}{R_{vd}}\right)\dfrac{V_{ref}}{C_{vf}}-\dfrac{V_{vf}}{C_{vf}R_{vf}}-\dfrac{V_0}{R_{vi}C_{vf}}=0, \\ \dfrac{(2fI_L(L_m+L_e)V_m-V_{in}V_{vf})L_e}{(2L_mV_{in}+2(L_m+L_e)NV_0+L_eV_{in})V_m}-D_2=0. \end{cases} \tag{11}$$

The Jacobian matrix for the improved averaged model at the equilibrium point is

$$J_{ac}=\begin{bmatrix} -\left(\dfrac{NV_0}{L_m}+\dfrac{V_{in}}{L_m+L_e}\right)\dfrac{\partial d_2}{\partial\langle i_L\rangle} & a_{12} & a_{13} \\ a_{21} & a_{22} & a_{23} \\ 0 & -\dfrac{1}{R_{vi}C_{vf}} & -\dfrac{1}{C_{vf}R_{vf}} \end{bmatrix}, \tag{12}$$

where

$$a_{12} = -\frac{N}{L_m}\left(1-\frac{V_{vf}}{V_m}+D_2\right) -\left(\frac{NV_0}{L_m}+\frac{V_{in}}{L_m+L_e}\right)\frac{\partial d_2}{\partial\langle v_0\rangle}, \tag{13}$$

$$a_{13} = \frac{NV_0}{L_mV_m}-\frac{NV_0}{L_m}\frac{\partial d_2}{\partial\langle v_{vf}\rangle} +\frac{V_{in}}{L_m+L_e}\left(\frac{1}{V_m}-\frac{\partial d_2}{\partial\langle v_{vf}\rangle}\right), \tag{14}$$

$$a_{21} = \frac{NI_L}{C}\left(1-\frac{V_{vf}}{V_m}+2D_2-\frac{V_{in}+NV_0}{2fL_eI_L}3D_2^2\right)\frac{\partial d_2}{\partial\langle i_L\rangle} +\frac{N}{C}\left(1-\frac{V_{vf}}{V_m}-\frac{V_{vf}}{V_m}D_2+D_2+D_2^2\right), \tag{15}$$

$$a_{22} = \frac{NI_L}{C}\left(1-\frac{V_{vf}}{V_m}+2D_2-\frac{V_{in}+NV_0}{2fL_eI_L}3D_2^2\right)$$

$$\times \frac{\partial d_2}{\partial \langle v_0 \rangle} - \frac{N^2 D_2^3}{2fCL_e} - \frac{1}{RC}, \tag{16}$$

$$a_{23} = \frac{NI_L}{C}\left(1 - \frac{V_{vf}}{V_m} + 2D_2 - \frac{V_{in} + NV_0}{2fL_eI_L}3D_2^2\right) \times \frac{\partial d_2}{\partial \langle v_{vf} \rangle} - \frac{NI_L(1+D_2)}{CV_m}, \tag{17}$$

$$\frac{\partial d_2}{\partial \langle i_L \rangle} = \frac{2f(L_m + L_e)V_mL_e}{(2L_mV_{in} + 2(L_m + L_e)NV_0 + L_eV_{in})V_m}, \tag{18}$$

$$\frac{\partial d_2}{\partial \langle v_0 \rangle} = \frac{(V_{in}V_{vf} - 2fI_L(L_m + L_e)V_m)(2(L_m + L_e)N)L_e}{(2L_mV_{in} + 2(L_m + L_e)NV_0 + L_eV_{in})^2V_m}, \tag{19}$$

$$\frac{\partial d_2}{\partial \langle v_{vf} \rangle} = \frac{-V_{in}L_e}{(2L_mV_{in} + 2(L_m + L_e)NV_0 + L_eV_{in})V_m}. \tag{20}$$

As shown in Refs. [18] and [19], if all the eigenvalues of the Jacobian matrix at the equilibrium point lie on the left side of the complex plane, the system will be in stable operation. Otherwise, the Hopf bifurcation will occur.

When taking $L_e = 168$ μH, the eigenvalues of the Jacobian matrix at different values of switching frequency f are calculated as shown in Table 1. It is found that when the switching frequency f is bigger than 18.9 kHz, i.e., $f >$ 18.9 kHz, all the eigenvalues lie on the left side of the complex plane, which implies that the system is in stable operation. However, when the switching frequency f is less than or equal to 18.9 kHz, i.e., $f \leq 18.9$ kHz, there is a pair of conjugate eigenvalues moving into the right side of the complex plane, which implies that the Hopf bifurcation occurs in the system so that the system loses its stability.

Table 1. Eigenvalues of Jacobian matrix at different values of switching frequency f for $L_e = 168$ μH.

f/kHz	λ_1	$\lambda_{2,3}$	State
50.0	–2696.1	–594.51±2023.9i	stable
40.0	–2457.4	–434.06±2268.4i	stable
30.0	–2288.2	–239.80±2471.9i	stable
20.0	–2163.6	–23.958±2635.8i	stable
19.0	–2152.9	–1.5152±2650.1i	stable
18.9	–2151.8	0.73640±2651.5i	unstable
10.0	–2067.9	205.774±2763.7i	unstable
6.00	–2035.4	300.445±2805.6i	unstable

Figure 3 shows at the stability boundary, which is obtained by noting down the critical values about the just, lose the stability in the voltage controlled flyback converter, the leakage inductance L_e versus switching frequency f. One can observe that the switching frequency f has an important effect on the stability of the voltage controlled flyback converter, i.e., the system stability region is enlarged by increasing the switching frequency f. However, in engineering applications, the higher switching frequency f will bring more switching loss, which leads to lower efficiency. Therefore, a compromise must be made when choosing the switching frequency f.

Furthermore, the leakage inductance L_e of the real transformer has also an important effect on the dynamical behaviors of the voltage controlled flyback converter, i.e., the system stability region is enlarged by increasing the leakage inductance L_e of the transformer. However, in practical engineering, the leakage inductance L_e of the transformer should be reduced to increase the utilization of the transformer for improving the efficiency. So, a compromise must also be made when choosing the value of leakage inductance L_e of the real transformer.

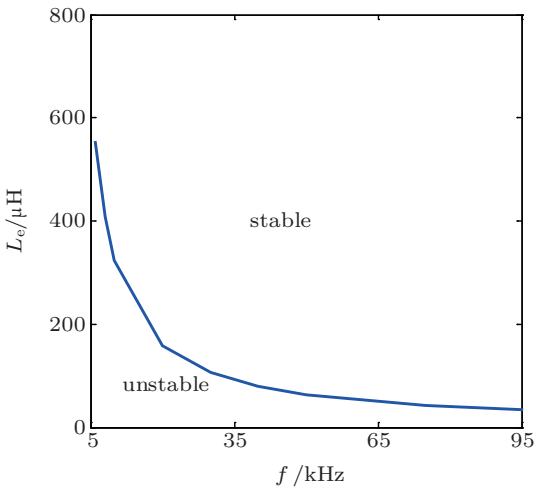


Fig. 3. (color online) Leakage inductance L_e at boundary versus switching frequency f.

4. Circuit simulations and experiments for verification

Here, the power electronics simulator (PSIM) software, which has been widely and effectively used to simulate the switching power converter and motor drives,[23,24] is used to simulate the voltage controlled flyback converter. Note that when the PSIM simulation is carried out, the results are displayed by using the PSIM software itself. Additionally, from Fig. 1, the hardware circuit of the voltage controlled flyback converter is designed, which is shown in Fig. 4. The switch S is realized by IRFP460, the diode D by MUR1560, the amplifier AM by LF356, the comparator COM by LM311, and a voltage sensor VSEN by INA111, which is a high speed FET-input instrumentation amplifier offering excellent performance. Additionally, the current probe Tektronix A622 is used to detect the current i_s, and the voltage probe Agilent 10074C is used to detect the output voltage v_0. The digital oscilloscope Agilent DSO-6014A is employed to capture the measured waveforms in the probes. Also, $V_{CC} = 15$ V, $R_D = 510$ Ω, and the other circuit parameters are shown in Section 2. Note that for the different circuit parameters, a large number of time-domain waveforms can be generated from the simulations and the circuit experiments. But only representative figures are shown here, which is used to exemplify the main findings.

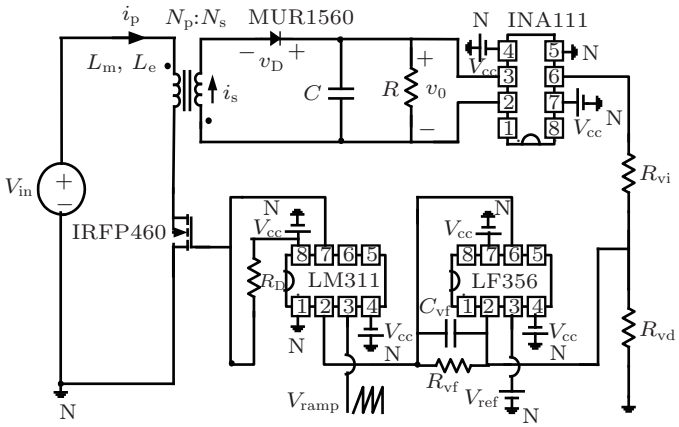


Fig. 4. Hardware circuit of the voltage controlled flyback converter.

For $f = 30$ kHz and $L_e = 168$ μH, the simulation results and the corresponding circuit experimental results are shown in Figs. 5 and 6, respectively. One can see that the simulation results are in good agreement with the circuit experimental results. Moreover, from Figs. 5 and 6, it is obvious that both the output voltage v_0 and the current i_S maintain the period-1 operation, implying that the system is in stable operation and these are in good agreement with the theoretical analysis in Section 3.

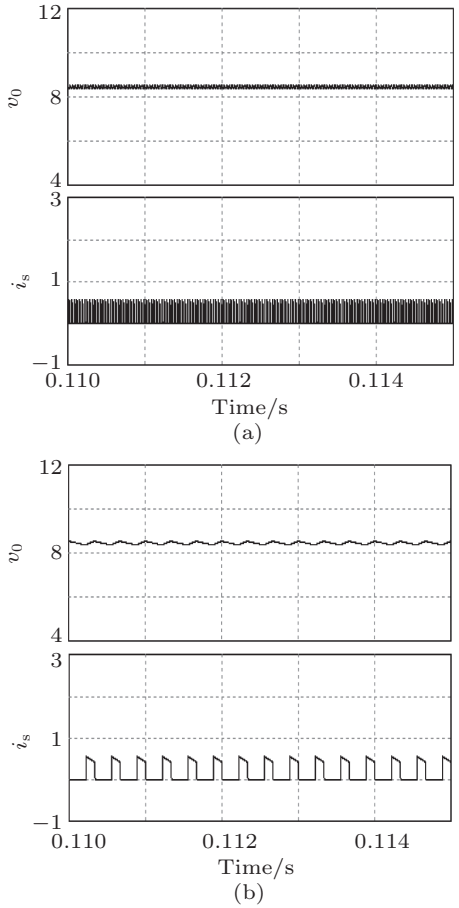


Fig. 5. Simulation results of (a) voltage v_0 and the current i_s, and (b) corresponding close-up view, for $f = 30$ kHz and $L_e = 168$ μH.

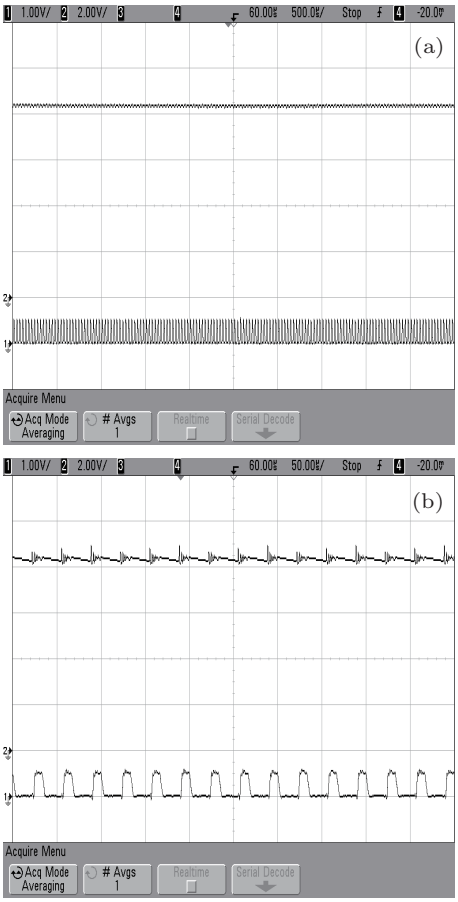


Fig. 6. Measured experimental waveforms of (a) voltage v_0 (upper trace: 2 V/div) and current i_s (lower trace: 1 V/div), time scale: 500 μs/div, and (b) the close-up view, time scale: 50 μs/div, for $f = 30$ kHz and $L_e = 168$ μH.

Moreover, when taking $f = 6$ kHz and $L_e = 168$ μH, the simulation results and the experimental results are shown in Figs. 7 and 8, respectively. One can see that the simulation results are also in good agreement with the circuit experimental results and they both show that, except for period-1 operation, they still display the oscillations whose frequencies are both approximate to 400 Hz, and accordingly the system loses its stability. It is also found that the amplitude of the output voltage and that of the diode current in this instability operation are larger than the ones in stable operation. Thus, the occurrence of this instability in the voltage controlled flyback converter cannot be accepted in practice. Note that the results from the simulations and experiments in this case are also in agreement with the theoretical analyses in Section 3.

Furthermore, the comparison between the theoretical analyses and simulation results about the stability boundaries is shown in Fig. 9. One can observe that the results for stability boundaries from these two ways are in good agreement with each other, and these show that the theoretical analysis in Section 3 is effective.

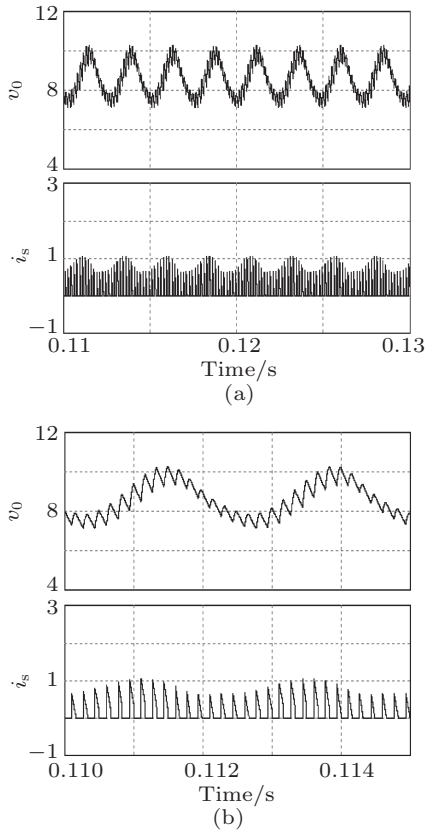


Fig. 7. Simulation results of (a) voltage v_0 and current i_s, and (b) corresponding close-up view for $f = 6$ kHz and $L_e = 168$ μH.

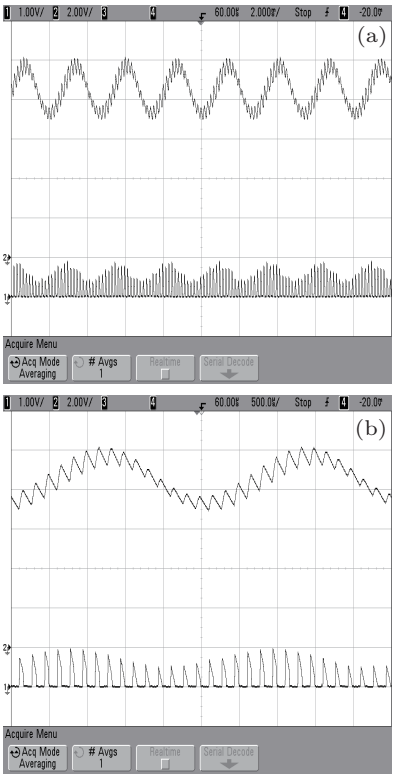


Fig. 8. Measured experimental waveforms of (a) voltage v_0 (upper trace: 2 V/div) and current i_s (lower trace: 1 V/div), time scale: 2 ms/div, and (b) close-up view, time scale: 500 μs/div, for $f = 6$ kHz and $L_e = 168$ μH.

Therefore, according to the above simulations, experiments and the corresponding comparisons, it is confirmed that the derived improved averaged model which covers the switching frequency f and the leakage inductance L_e is an effective model to analyze their important effects on the slow-scale stability in the voltage controlled flyback converter.

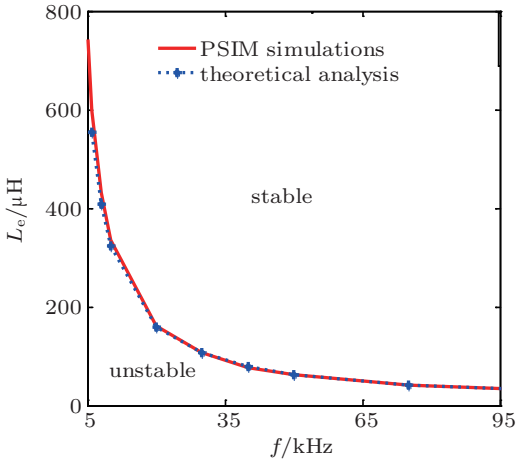


Fig. 9. (color online) Comparison between the theoretical analyses and the PSIM simulations about the stability boundaries.

5. Conclusions

The flyback converter as a primary isolated switching power converter has been widely used in low power applications. Based on the derived improved averaged model which covers the switching frequency f and the leakage inductance L_e, the effects of these two circuit parameters on the slow-scale stability in the voltage controlled flyback converter are investigated in this paper. The results among the PSIM simulations, the theoretical analysis, and the circuit experiment are in good agreement with each other and the following main findings are obtained:

(i) The derived improved averaged model is an effective model for analyzing the effects of the switching frequency f and the leakage inductance L_e on slow-scale stability in the voltage controlled flyback converter.

(ii) The Hopf bifurcation occurs in some parameter values and it mainly leads to the voltage controlled flyback converter losing its slow-scale stability.

(iii) A compromise must be made when choosing the switching frequency f since its higher value leads to the larger stability region but with a lower efficiency.

(iv) A compromise must be made when choosing the leakage inductance L_e since its higher value leads to the larger stability region but with a lower utilization of the transformer.

References

[1] Lee M C, Lio J B, Chen D Y, Chen Y T and Wu Y P 1998 *IEEE Trans. Ind. Electron.* **45** 236

[2] Chen T H, Lin W L and Liaw C M 1999 *IEEE Trans. Aerospace Electron. Syst.* **35** 1230

[3] Telefus M, Shteynberg A, Ferdowsi M and Emadi A 2004 *IEEE Trans. Power Electron.* **19** 757
[4] Suntio T 2006 *IEEE Trans. Power Electron.* **21** 479
[5] Liang T J and Tseng K C 2005 *IEE Proc. Electr. Power Appl.* **152** 217
[6] Murthy-Bellur D and Kazimierczuk M K 2011 *Int. J. Circ. Theor. Appl.* **39** 1145
[7] Murthy-Bellur D and Kazimierczuk M K 2011 *Int. J. Circ. Theor. Appl.* **39** 849
[8] Birca-Galateanu S 1987 *IEEE Trans. Aerospace Electron. Syst.* AES-**23** 146
[9] Hsieh F H, Lin K M and Su J H 2009 *Proceedings of 4th IEEE Conference on Industrial Electronics and Applications*, May 25–27, 2009, Xi'an, China, p. 166
[10] Xie F, Yang R and Zhang B 2011 *IEEE Trans. Circ. Syst. I* **58** 2269
[11] Wang F Q and Ma X K 2011 *Phys. Lett. A* **375** 1451
[12] El Aroudi A, Benadero L, Toribio E and Machiche S 2000 *Int. J. Bifur. Chaos* **10** 359
[13] Maity S, Tripathy D, Bhattacharya T K and Banerjee S 2007 *IEEE Trans. Circ. Syst. I* **54** 1120
[14] El Aroudi A, Benadero L, Toribio E and Olivar G 1999 *IEEE Trans. Circ. Syst. I* **46** 1374
[15] Wang J P, Xu J P, Zhou G H, Mi C B and Qin M 2011 *Acta Phys. Sin.* **60** 048402 (in Chinese)
[16] Ma W, Wang M Y and Nie H L 2011 *Acta Phys. Sin.* **60** 100202 (in Chinese)
[17] Iu H H C, Tse C K, Pjevalica V and Lai Y M 2001 *Int. J. Circ. Theor. Appl.* **29** 281
[18] Tse C K, Lai Y M and Iu H H C 2000 *IEEE Trans. Circ. Syst. I* **47** 448
[19] Iu H H C and Tse C K 2003 *IEEE Trans. Circ. Syst. I* **50** 679
[20] Chen Y F, Tse C K, Qiu S S, Lindenmuller L and Schwarz W 2008 *IEEE Trans. Circ. Syst. I* **55** 3335
[21] Wong S C, Wu X Q and Tse C K 2008 *IEEE Trans. Circ. Syst. II* **55** 489
[22] Witulski A F 1995 *IEEE Trans. Power Electron.* **10** 349
[23] Onoda S and Emadi A 2004 *IEEE Trans. Veh. Technol.* **53** 390
[24] PSIM Version 9.0. Powersim Inc.